Applied Physics Letters ARTICLE pubs.aip.org/aip/apl

Structural, electronic, and superconducting properties of MBE-grown tantalum nitride films on c-plane sapphire

Cite as: Appl. Phys. Lett. **126**, 222601 (2025); doi: 10.1063/5.0267713
Submitted: 25 February 2025 · Accepted: 13 May 2025 ·
Published Online: 4 June 2025

Anand Ithepalli,[1] Amit Rohan Rajapurohita,[2] Arjan Singh,[3] Rishabh Singh,[2] John Wright,[1] Farhan Rana,[3] Valla Fatemi,[2] Huili (Grace) Xing,[1,3,4] and Debdeep Jena[1,3,4,a)]

AFFILIATIONS

[1]Department of Materials Science and Engineering, Cornell University, Ithaca, New York 14850, USA
[2]School of Applied and Engineering Physics, Cornell University, Ithaca, New York 14850, USA
[3]School of Electrical and Computer Engineering, Cornell University, Ithaca, New York 14850, USA
[4]Kavli Institute at Cornell for Nanoscale Science, Cornell University, Ithaca, New York 14850, USA

[a)]Author to whom correspondence should be addressed: djena@cornell.edu

ABSTRACT

Two single crystal phases of tantalum nitride were stabilized on c-plane sapphire using molecular beam epitaxy. The phases were identified to be δ-TaN with a rock salt cubic structure and γ-Ta_2N with a hexagonal structure. Atomic force microscopy scans revealed smooth surfaces for both the films with root mean square roughnesses less than 0.3 nm. Phase purity of these films was determined by x-ray diffraction. The Raman spectrum of the phase-pure δ-TaN and γ-Ta_2N obtained will serve as a future reference to determine phase purity of tantalum nitride films. Furthermore, the room temperature and low-temperature electronic transport measurements indicated that both of these phases are metallic at room temperature with resistivities of 586.2 $\mu\Omega \cdot$ cm for the 30 nm δ-TaN film and 75.5 $\mu\Omega \cdot$ cm for the 38 nm γ-Ta_2N film and become superconducting below 3.6 and 0.48 K, respectively. The superconducting transition temperature reduces with applied magnetic field as expected. Ginzburg–Landau fitting revealed a 0 K critical magnetic field and coherence length of 18 T and 4.2 nm for the 30 nm δ-TaN film and 96 mT and 59 nm for the 38 nm γ-Ta_2N film. These tantalum nitride films are of high interest for superconducting resonators and qubits.

Tantalum (Ta) metal has gained significant attention within the superconducting resonator community due to the long lifetimes of about 0.3 ms for Ta-based qubits[1] and the high quality factors in Ta co-planar waveguide (CPW) resonators, especially at low photon numbers.[2] The reason behind the success of Ta in this field is still being investigated. The primary hypothesis is that the native oxide of Ta, Ta_2O_5, is not only the most stable native oxide of Ta but also aggressive acid treatment can selectively remove this oxide and other contaminants without affecting the Ta metal.[3] This motivates us to investigate tantalum nitride, which should reduce the surface oxide even more due to the presence of Ta–N bonds. To test whether tantalum nitride films can improve the state-of-the-art resonator quality factors, it is important to deposit these films with the least amount of defects on a low-dielectric loss substrate like sapphire (Al_2O_3). Molecular beam epitaxy (MBE) as a deposition technique specializes in these extreme requirements and has also seen success over other deposition techniques in the superconducting resonator field in the recent past.[4–7] With this motivation, we developed the growth conditions for stabilizing single crystal, phase-pure tantalum nitride films on c-plane sapphire by MBE. In particular, the phases stabilized are a rock salt δ-TaN phase, which has the highest superconducting critical temperature among all the tantalum nitride phases, and a hexagonal γ-Ta_2N phase, which is symmetry matched to the conventional III-nitrides with wurtzite structure.

The tantalum metal source with a purity of 99.95% was evaporated using an e-beam source connected to the Veeco GenXplor MBE system with a base pressure below 10^{-10} Torr and the active nitrogen flux was generated using a radio frequency plasma source connected to a 6N5 pure N_2 gas. Wright *et al.* identified 200 W plasma power and 2 sccm (cubic centimeter per minute at standard temperature and pressure) nitrogen flow rate as the nitrogen plasma conditions to stabilize all the niobium nitride phases,[8] this corresponds to roughly 2:1

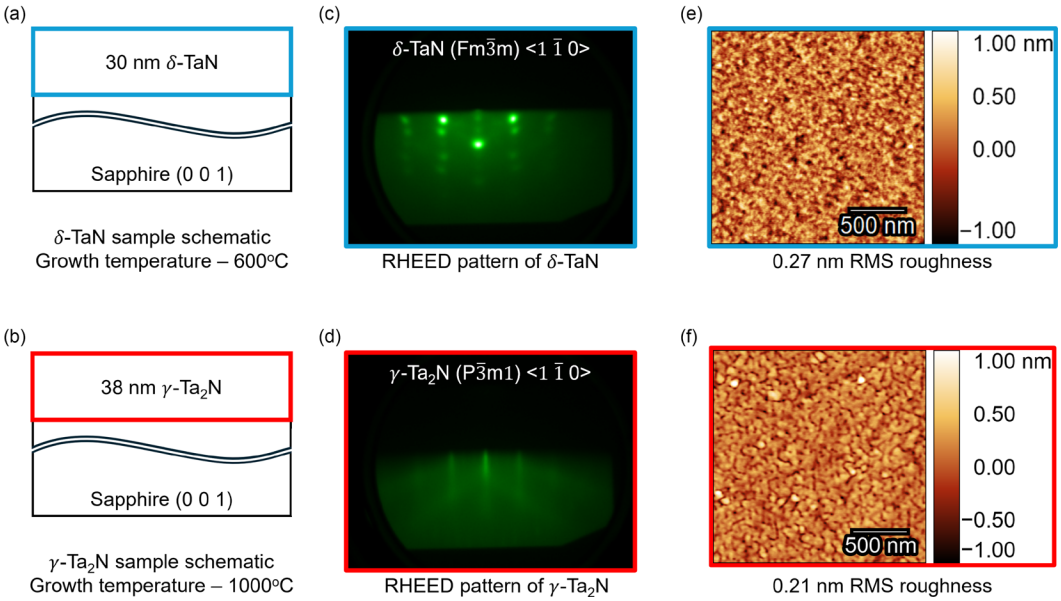

FIG. 1. (a) and (b) Sample schematics of 30 nm δ-TaN and 38 nm γ-Ta_2N films, respectively. (c) and (d) RHEED patterns after the growth of the films shown in (a) and (b) with the space groups of the films and zone axes indexed according to the film orientations. These RHEED patterns indicate single crystal twinned, three-dimensional growth mode of δ-TaN and single crystal, two-dimensional growth mode of γ-Ta_2N. (e) and (f) Atomic force microscopy (AFM) scans of the films shown in (a) and (b) indicate that both the films have smooth surfaces with root mean square (RMS) roughnesses below 0.3 nm.

ratio of active nitrogen:metal flux. While these plasma conditions were enough to stabilize γ-Ta_2N phase, the δ-TaN phase required 450 W and 3 sccm plasma conditions, corresponding to a 5:1 active nitrogen: metal flux ratio, probably due to reduced nitrogen diffusivity in tantalum compared to that in niobium. During growth, the chamber pressure was around 2×10^{-5} Torr. The schematics of the two samples used in this study are shown in Figs. 1(a) and 1(b). The sample in Fig. 1(a) was grown at a substrate temperature of 600 °C as measured by a thermocouple near the heater. After a 15 min growth, the thickness as measured by x-ray reflectivity was 30 nm. Similarly, the sample in Fig. 1(b) was grown at a substrate temperature of 1000 °C. The thickness of this film was determined to be 38 nm.

The reflection high energy electron diffraction (RHEED) patterns of the tantalum nitride films of Figs. 1(a) and 1(b) are shown in Figs. 1(c) and 1(d), respectively. The RHEED patterns indicate that the surface of the sample grown at 600 °C has a twinned cubic structure with a three-dimensional growth mode represented by spotty RHEED pattern. This corresponds to the δ-TaN phase with an Fm$\bar{3}$m space group. This is very similar to niobium nitride grown at the same temperature in the same system as reported by Wright *et al.*[8] Similar to the high temperature growths of niobium nitride by Wright *et al.*, the RHEED pattern of the film grown at 1000 C indicates a two-dimensional growth mode.[8] This phase was later identified as the γ-Ta_2N phase with a P$\bar{3}$m1 space group. We note that this hexagonal phase is directly analogous to β-Nb_2N, see Refs. 8 and 9 (it is referred to as γ-Ta_2N because of the presence of a β-Ta allotrope, the corresponding phase of which is absent for Nb). The fact that the growth temperature has a larger impact on the film stoichiometry than the nitrogen plasma conditions and the nitrogen to metal flux ratio implies that the growth kinetics are limited by the nitrogen desorption rate from the crystal, which is strongly determined by the substrate temperature following the Arrhenius law.

Atomic force microscopy (AFM) scans of both the films in Figs. 1(a) and 1(b) shown in Figs. 1(e) and 1(f), respectively, indicate that both the films were very smooth with a root mean square roughness of less than 0.3 nm. However, the AFM features observed were not in accordance with the corresponding results of niobium nitride from Wright *et al.*[8] For example, the atomic steps were not observed in the high temperature phase of tantalum nitride. The step flow growth mode of the γ-Ta_2N phase may be expected at even higher growth temperatures.

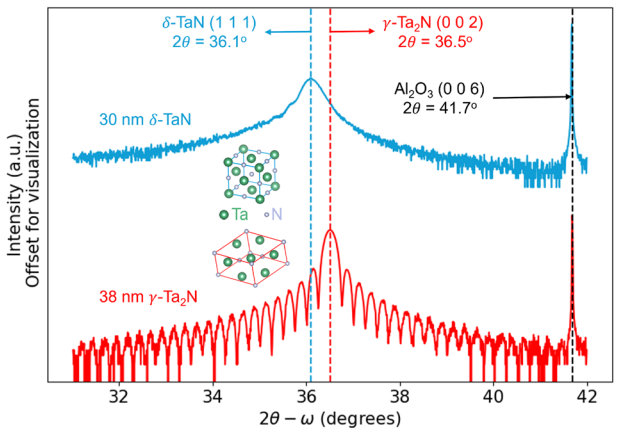

FIG. 2. Singular peaks of the symmetric 2θ-ω coupled scans of the 30 nm δ-TaN and 38 nm γ-Ta_2N films indicating the single crystal nature of these films.

Figure 2 shows the symmetric x-ray diffraction (XRD) scans of both the δ-TaN and γ-Ta_2N films. The y-axis of the scans is in log scale with the peak intensity being 1000 times the noise floor The scans were offset for visualization. The XRD data indicate the presence of only one phase in each of these samples. These peak positions were matched with the bulk tantalum nitride XRD data to identify the phase and orientation of the crystals with respect to sapphire substrate. The crystal structures thus identified are represented on Fig. 2 close to the corresponding scan. The (1 1 1) orientation of δ-TaN and (0 0 2) orientation of γ-Ta_2N were identified as expected from the niobium nitride results by Wright *et al.*[8] The Pendellösung fringes are clearer and significantly more in the case of γ-Ta_2N compared to that of δ-TaN. This is also consistent with the XRD results from niobium nitride.[8]

Reciprocal space maps (RSMs), as presented in Fig. 3, were used to further determine the phase purity of these films. The scans were all performed with the [1 0 0] axis of sapphire being parallel to the x-ray beam path. This means that the planes of tantalum nitride films and sapphire substrate detected in the measurement share the sapphire [1 $\bar{1}$ 0] zone axis. Figure 3(a) shows the legend of the planes of each of the phases we looked for. Figures 3(b) and 3(c) show the RSMs of the planes shown in Fig. 3(a) for the δ-TaN and γ-Ta_2N films as indicated by the inset schematics.

In Fig. 3(b), only the TaN (1 3 3) plane is observed in addition to the sapphire (1 1 9) plane indicating phase-pure δ-TaN. Similarly, only the Ta_2N (1 0 5) plane is observed in addition to the sapphire (1 1 9) plane in Fig. 3(c) indicating phase-pure γ-Ta_2N. The unit cells and the colored planes shown in the insets of Figs. 3(b) and 3(c) are based on the crystal symmetry and the measured planes, respectively, and are not to scale.

Based on the x-ray diffraction data, the lattice constant of the δ-TaN film was extracted to be $a = 4.306$ Å. This is very close to the bulk lattice constant $a = 4.331$ Å of rock salt cubic δ-TaN given by Gatterer *et al.*[10] [ICSD-76456]. Similarly, the lattice constants of γ-Ta_2N are extracted as $a = 3.060$ Å and $c = 4.919$ Å, which also match the bulk γ-Ta_2N lattice constants of $a = 3.0476$ Å and $c = 4.9187$ Å given by Brauer *et al.*[11] [ICSD-76015].

It must be noted that the Ta-N equilibrium phase diagram is very similar to but a little bit more complicated than the Nb-N phase diagram due to the increased covalent nature of the Ta–N bonds.[9,12] This leads to a wide range of Ta:N stoichiometries being stable with different crystal structures. Each of these crystal structures will have their own orientation corresponding to the sapphire substrate. In Fig. 3, we only looked for the tantalum nitride phases whose orientations with respect to sapphire were understood from niobium nitride phases. Nevertheless, the singular peaks in XRD scans shown in Fig. 2 along with RSMs shown in Fig. 3 indicate phase purity in both the films.

Figure 4 shows the Raman spectra of the δ-TaN and γ-Ta_2N films collected using a WITec alpha300 Raman microscope with a pump laser wavelength of 532 nm at room temperature. Raman spectra of superconducting refractory metals has long been investigated to understand the relationship between phonon density and superconducting transition temperature (see, e.g., Ref. 13) Such studies in niobium nitride revealed a distinct Raman signature associated with each phase.[13] Raman spectroscopy can thus be used to determine phase purity of samples from material systems with complex phase diagrams such as tantalum nitride and niobium nitride. As can be seen in Fig. 4, our δ-TaN and γ-Ta_2N films also exhibit significantly different Raman spectra, given the differences in both crystal structure and stoichiometry between the phases. The Raman spectra and the corresponding peak positions that we report here (Fig. 4) may be used as reference for phase-pure δ-TaN and γ-Ta_2N. Note that the broad band of peaks between 100 and 200 cm^{-1} for δ-TaN is similar to that of δ-NbN reported in Ref. 13.

The temperature-dependent electrical resistivity of the δ-TaN and γ-Ta_2N films was measured using a four probe method in a Quantum Design Dynacool physical properties measurement system (PPMS). An additional He-3 option, capable of reaching 0.36 K, was

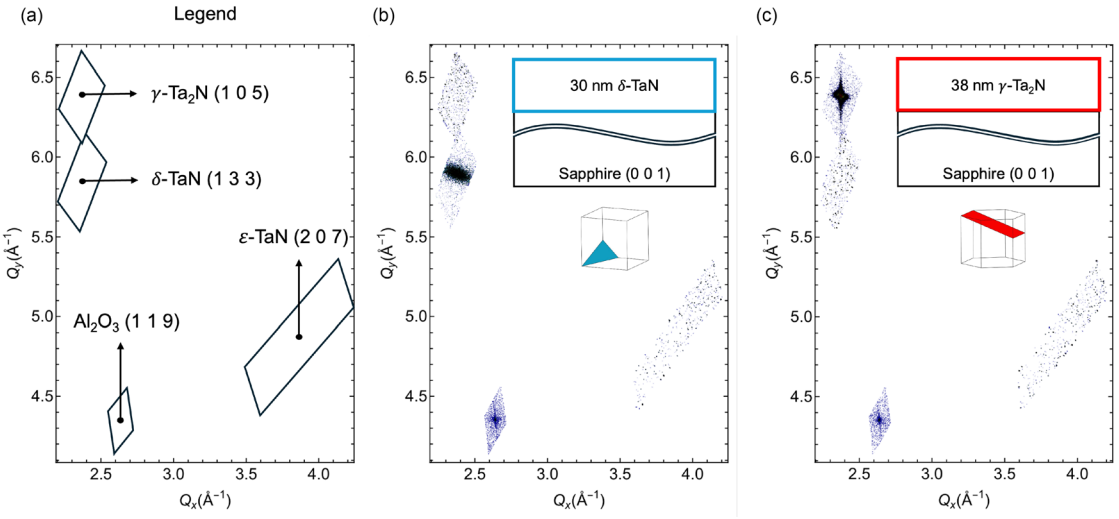

FIG. 3. Reciprocal space mapping (RSM) figures are used to verify the presence of multiple phases and orientations of the films with respect to the substrate. (a) Legend of the expected peak locations of the tantalum nitride phases of interest alongside a sapphire substrate asymmetric peak. All the RSM figures shown here have planes corresponding to ⟨ 1 0 9 ⟩ zone axis of the sapphire substrate. (b) RSM figure of δ-TaN and (c) RSM figure of γ-Ta_2N indicating the presence of only intended phases.

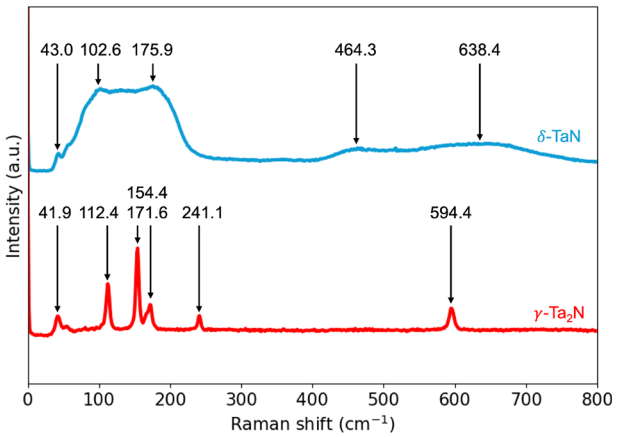

FIG. 4. Raman spectra of the 30 nm δ-TaN and 38 nm γ-Ta_2N films. The peaks in Raman spectra, which are unique to each phase of tantalum nitride, can be used to identify the phases present in a film.

used to observe superconductivity in γ-Ta_2N. The resistivity vs temperature data are shown in Fig. 5. The resistivity of the δ-TaN film is 10 times the value indicated by the y axis. This scaling allows us to compare both the films in one plot. A direct comparison to the literature for the δ-TaN film shown in this work is difficult due to its differences in the thickness, deposition technique, substrate, etc. However, the reported room temperature resistivity values in the literature are between 74 and few thousand $\mu\Omega \cdot$ cm,[16,17] as tabulated in Table I. Such a large range is due to the frequently observed metal to insulator transition in tantalum nitride films. The room temperature resistivity of our 30 nm δ-TaN film is 586.2 $\mu\Omega \cdot$ cm and falls in the same range. On the contrary, the room temperature resistivity of our 38 nm γ-Ta_2N film is 75.5 $\mu\Omega \cdot$ cm and is comparable to the 66 $\mu\Omega \cdot$ cm for a 43 nm MBE-grown γ-Ta_2N film on SiC reported in Ref. 9.

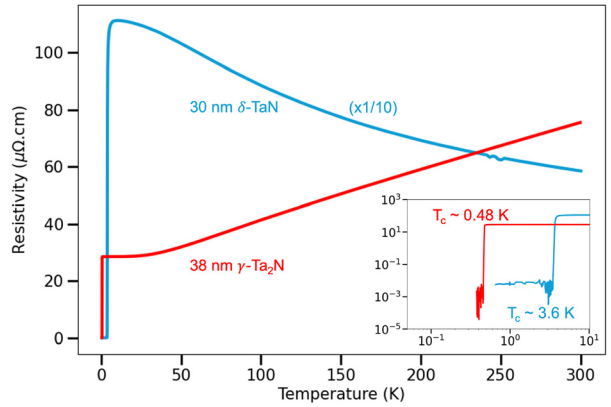

FIG. 5. Temperature dependent resistivity (ρ vs T) measurements of the 30 nm δ-TaN and 38 nm γ-Ta_2N films. ρ vs T of 30 nm δ-TaN is multiplied by 1/10 to have the plots in the same scale. The actual room temperature resistivities are 586.2 $\mu\Omega$. cm for the 30 nm δ-TaN film and 75.5 $\mu\Omega$.cm for the 38 nm γ-Ta_2N film. (Inset) The log–log plot of ρ vs T showing a superconducting transition at around 3.6 K for the 30 nm δ-TaN film and 0.48 K for the 38 nm γ-Ta_2N film.

The residual resistivity ratio (RRR), defined as $\rho_{300\,K}/\rho_{10\,K}$, of the δ-TaN film is 0.52, which is less than unity, similar to the RRR of δ-NbN, as reported by Wright *et al.*[8] For the γ-Ta_2N film, the RRR is 2.6, similar to the RRR of β-Nb_2N.[8] The inset of Fig. 5 shows the superconducting transition in both the films. δ-TaN has a superconducting transition temperature (T_c) $\simeq$ 3.6 K, although δ-TaN has been shown to have T_c as high as 10.8 K in a 300 nm TaN film sputter deposited on molybdenum substrate at room temperature.[18] This is possibly due to low-temperature growth, lower thickness, and phase purity of our film. The mixed phases have been shown to possess the highest T_c in the niobium nitride family on both sapphire and SiC substrates.[8,19] Moreover, the $T_c \simeq$ 3.6 K of our 30 nm δ-TaN film is very close to the $T_c \simeq$ 3.7 K of δ-TaN film of similar thickness reported previously.[14] γ-Ta_2N has a $T_c \simeq$ 0.48 K very similar to that of β-Nb_2N.[8] The previous MBE-grown γ-Ta_2N by Katzer *et al.*, was shown to have higher T_c at the expense of phase mixture.[9]

We measured the T_c under a range of magnetic fields perpendicular to the surface of both the films as shown in Figs. 6 and 7. The T_c was extracted to be the temperature at which the resistance drops to 90% of the normal state resistance just above the transition temperature. The magnetic field-dependent normalized ρ vs T curves and the corresponding 90% lines are shown as insets in Figs. 6 and 7. The linearized Ginzburg–Landau (GL) fit is given by

$$B_{c2}^{\perp}(T) = \frac{\phi_0}{2\pi\xi^2}\left(1 - \frac{T}{T_c}\right), \tag{1}$$

where $\phi_0 = h/2e$ is the magnetic flux quantum, a ratio of the fundamental constants—Planck's constant h and fundamental charge e. The factor of 2 in front of e is due to the Cooper pairs in superconductors. $B_{c2}^{\perp}(T)$ is the upper critical field perpendicular to the film at a given temperature T, and $\xi = \xi_{GL}(0\,K)$ is the GL coherence length at 0 K.

Equation (1) was then used to extract the 0 K GL coherence length, ξ_{GL}, and the 0 K critical magnetic field, B_{c2}, similar to Yan *et al.*[20] Both the linear GL fits shown in Figs. 6 and 7 had > 99% r-squared value, indicating a good fit. The extracted values are $\xi_{GL}(0\,K) \simeq$ 4.2 nm and $B_{c2}(0\,K) \simeq$ 18 T for the 30 nm δ-TaN film. The previously reported $B_{c2}(0\,K)$ of 13.8 T matches closely with our results.[21] Similar to the structural properties, the $B_{c2}(0\,K)$ of 30 nm TaN film matches that of the values of delta niobium nitride thin film with much higher $T_c \simeq$ 16 K reported by Dang *et al.*[22] $\xi_{GL}(0\,K) \simeq$ 59 nm and $B_{c2}(0\,K) \simeq$ 96 mT are extracted for 38 nm γ-Ta_2N film. GL analysis was also performed with critical temperature defined by 10% of the normal state resistance just above the transition temperature. This resulted in a 13 T critical magnetic field, a 5.1 nm GL coherence length for the δ-TaN film, a 77 mT critical magnetic field, and a 66 nm GL coherence length for the γ-Ta_2N film.

In conclusion, growth conditions were identified for obtaining two single crystal, phase-pure tantalum nitride phases on c-plane sapphire by tuning the growth temperature and the Ta metal flux. The phase purity of these films was identified from x-ray measurements. The temperature-dependent electronic measurements were then performed on these films to identify crucial superconducting parameters like critical temperature, critical magnetic field, and GL coherence lengths. Moving forward, we anticipate realization of superconducting resonators from MBE-grown phase-pure single crystal tantalum nitride films. Theoretical and experimental assessment of the evolution

TABLE I. Electronic properties of δ-TaN and γ-Ta_2N thin films from various works compared with this study.

Film	Substrate	Deposition technique	Film thickness (nm)	Room temperature resistivity ($\mu\Omega$.cm)	Superconducting critical temperature (K)	Ref.
δ -TaN	c-Sapphire	MBE	30	586.2	3.6	This work
δ -TaN	Si, glass	Sputtering	36	1800	3.7	14
δ -TaN	MgO	Sputtering	10	74	5.6	15
δ -TaN	Al_2O_3+SiC	Sputtering	50–100	$\sim$1000	...	16
TaN_x	MgO	Sputtering	7–40	400 to 4×10^5	...	17
γ -Ta_2N	c-Sapphire	MBE	38	75.5	0.48	This work
γ -Ta_2N	SiC	MBE	43	66	1.25	9

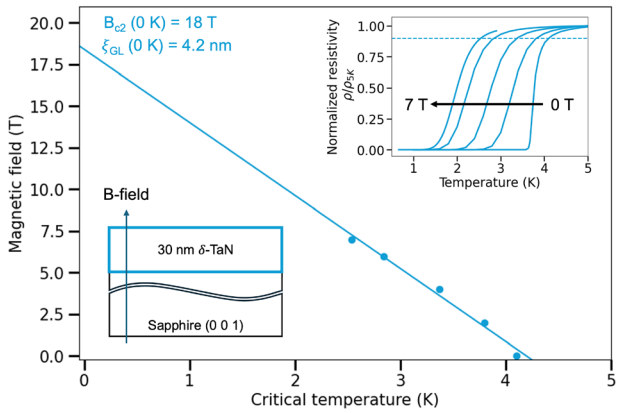

FIG. 6. Superconducting transition temperatures of the 30 nm δ-TaN film, taken as the temperatures where the resistance value drops to 90% of the normal state value at 5 K, extracted at various applied perpendicular magnetic fields [0 T, 2 T, 4 T, 6 T, 7 T] were fit using linearized Ginzburg–Landau (GL) formula. This linear GL fit resulted in a 0 K critical field of 18.4 T and GL coherence length of 4.23 nm. (Inset) ρ vs T curves normalized to the ρ value at 5 K.

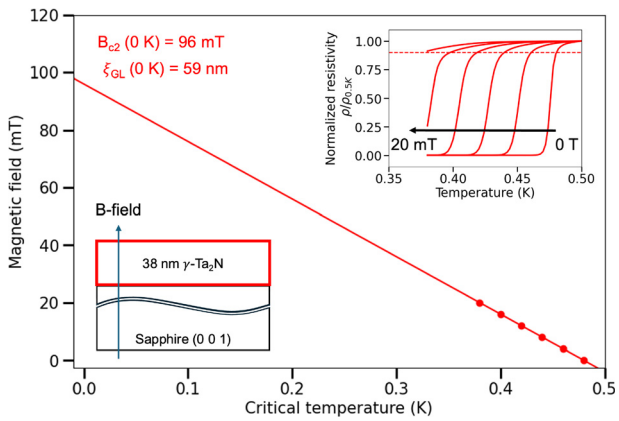

FIG. 7. Superconducting transition temperatures of the 38 nm γ-Ta_2N film, taken as the temperatures where the resistance value drops to 90% of the normal state value at 0.5 K, extracted at various applied perpendicular magnetic fields [0, 4, 8, 12, 16, 20 mT] were fit using linearized Ginzburg–Landau (GL) formula. This linear GL fit resulted in a 0 K critical field of 96 mT and a GL coherence length of 58.6 nm. (Inset) ρ vs T curves normalized to the ρ value at 0.5 K.

of Ta–N bonds at the surfaces in the presence of atmospheric oxygen will greatly support future work on the tantalum nitride platform.

This work was supported by the AFOSR/LPS program Materials for Quantum Computation (MQC) as part of the EpiQ team monitored by Dr. Ali Sayir of AFOSR and Dr. Erin Cleveland of LPS, and partially by an ONR Grant No. N00014-22-1-2633 monitored by Dr. Paul Maki. This material is based upon work supported by the Air Force Office of Scientific Research under Award No. FA9550-23-1-0688. Any opinions, findings, and conclusions or recommendations expressed in this material are those of the author(s) and do not necessarily reflect the views of the United States Air Force. This work was performed in part at the Cornell NanoScale Facility, a member of the National Nanotechnology Coordinated Infrastructure (NNCI), which is supported by the National Science Foundation (Grant No. NNCI-2025233). The authors acknowledge the use of facilities and instrumentation supported by NSF through the Cornell University Materials Research Science and Engineering Center DMR-1719875.

AUTHOR DECLARATIONS

Conflict of Interest

The authors have no conflicts to disclose.

Author Contributions

Anand Ithepalli: Conceptualization (equal); Data curation (equal); Formal analysis (equal); Investigation (equal); Methodology (equal); Visualization (equal); Writing – original draft (equal). **Amit Rohan Rajapurohita:** Investigation (supporting). **Arjan Singh:** Data curation (supporting); Investigation (supporting); Visualization (supporting); Writing – original draft (supporting). **Rishabh Singh:** Investigation (supporting); Writing – review & editing (supporting). **John Wright:** Investigation (supporting); Visualization (supporting). **Farhan Rana:** Funding acquisition (supporting); Supervision (supporting); Validation (supporting); Writing – review & editing (supporting). **Valla Fatemi:** Funding acquisition (supporting); Supervision (supporting); Validation (supporting); Writing – review & editing (equal). **Huili (Grace) Xing:** Funding acquisition (supporting); Supervision (supporting); Validation (supporting); Writing – review & editing (equal). **Debdeep Jena:** Conceptualization (equal); Funding acquisition (equal); Supervision (equal); Validation (equal); Writing – review & editing (equal).

DATA AVAILABILITY

The data that support the findings of this study are available from the corresponding author upon reasonable request.

REFERENCES

[1]A. P. Place, L. V. Rodgers, P. Mundada, B. M. Smitham, M. Fitzpatrick, Z. Leng, A. Premkumar, J. Bryon, A. Vrajitoarea, S. Sussman *et al.*, "New material platform for superconducting transmon qubits with coherence times exceeding 0.3 milliseconds," Nat. Commun. **12**, 1779 (2021).

[2]K. D. Crowley, R. A. McLellan, A. Dutta, N. Shumiya, A. P. M. Place, X. H. Le, Y. Gang, T. Madhavan, M. P. Bland, R. Chang, N. Khedkar, Y. C. Feng, E. A. Umbarkar, X. Gui, L. V. H. Rodgers, Y. Jia, M. M. Feldman, S. A. Lyon, M. Liu, R. J. Cava, A. A. Houck, and N. P. de Leon, "Disentangling losses in tantalum superconducting circuits," Phys. Rev. X **13**, 041005 (2023).

[3]R. A. McLellan, A. Dutta, C. Zhou, Y. Jia, C. Weiland, X. Gui, A. P. M. Place, K. D. Crowley, X. H. Le, T. Madhavan, Y. Gang, L. Baker, A. R. Head, I. Waluyo, R. Li, K. Kisslinger, A. Hunt, I. Jarrige, S. A. Lyon, A. M. Barbour, R. J. Cava, A. A. Houck, S. L. Hulbert, M. Liu, A. L. Walter, and N. P. de Leon, "Chemical profiles of the oxides on tantalum in state of the art superconducting circuits," Adv. Sci. **10**, 2300921 (2023).

[4]A. Megrant, C. Neill, R. Barends, B. Chiaro, Y. Chen, L. Feigl, J. Kelly, E. Lucero, M. Mariantoni, P. J. J. O'Malley, D. Sank, A. Vainsencher, J. Wenner, T. C. White, Y. Yin, J. Zhao, C. J. Palmstrøm, J. M. Martinis, and A. N. Cleland, "Planar superconducting resonators with internal quality factors above one million," Appl. Phys. Lett. **100**, 113510 (2012).

[5]G. A. Olson, "Growth of titanium-nitride thin films for low-loss superconducting quantum circuits," Ph.D. thesis (University of Illinois at Urbana-Champaign, 2015).

[6]C. J. K. Richardson, A. Alexander, C. G. Weddle, B. Arey, and M. Olszta, "Low-loss superconducting titanium nitride grown using plasma-assisted molecular beam epitaxy," J. Appl. Phys. **127**, 235302 (2020).

[7]C. R. H. McRae, H. Wang, J. Gao, M. R. Vissers, T. Brecht, A. Dunsworth, D. P. Pappas, and J. Mutus, "Materials loss measurements using superconducting microwave resonators," Rev. Sci. Instrum. **91**, 091101 (2020).

[8]J. G. Wright, H. G. Xing, and D. Jena, "Growth windows of epitaxial NbN_x films on c-plane sapphire and their structural and superconducting properties," Phys. Rev. Mater. **7**, 074803 (2023).

[9]D. S. Katzer, N. Nepal, M. T. Hardy, B. P. Downey, D. F. Storm, E. N. Jin, R. Yan, G. Khalsa, J. Wright, A. C. Lang, T. A. Growden, V. Gokhale, V. D. Wheeler, A. R. Kramer, J. E. Yater, H. G. Xing, D. Jena, and D. J. Meyer, "Molecular beam epitaxy of transition metal nitrides for superconducting device applications," Phys. Status Solidi A **217**, 1900675 (2020).

[10]J. Gatterer, G. Dufek, P. Ettmayer, and R. Kieffer, "Das kubische Tantalmononitrid (B 1-Typ) und seine Mischbarkeit mit den isotypen Übergangsmetallnitriden und-carbiden," Monatsh. Chem. **106**, 1137 (1975).

[11]G. Brauer and K. H. Zapp, "Die Nitride des Tantals," Z. Anorg. Allg. Chem. **277**, 129 (1954).

[12]N. Terao, "Structure of tantalum nitrides," Jpn. J. Appl. Phys., Part 1 **10**, 248 (1971).

[13]R. Kaiser, W. Spengler, S. Schicktanz, and C. Politis, "Raman spectra and superconductivity of various phases of a high-Tc superconductor: NbN," Phys. Status Solidi B **87**, 565 (1978).

[14]N. P. Breznay, M. Tendulkar, L. Zhang, S.-C. Lee, and A. Kapitulnik, "Superconductor to weak-insulator transitions in disordered tantalum nitride films," Phys. Rev. B **96**, 134522 (2017).

[15]P. W. Swatek, X. Hang, Y. Fan, W. Jiang, H. Yun, D. Lyu, D. Zhang, T. J. Peterson, P. Sahu, O. J. Benally, Z. Cresswell, J. Liu, R. Pahari, D. Kukla, T. Low, K. A. Mkhoyan, and J.-P. Wang, "Room temperature spin-orbit torque efficiency in sputtered low-temperature superconductor δ-tan," Phys. Rev. Mater. **6**, 074206 (2022).

[16]D. K. Kim, H. Lee, D. Kim, and Y. Keun Kim, "Electrical and mechanical properties of tantalum nitride thin films deposited by reactive sputtering," J. Cryst. Growth **283**, 404 (2005).

[17]A. B. Kaul, S. R. Whiteley, T. Van Duzer, L. Yu, N. Newman, and J. M. Rowell, "Internally shunted sputtered NbN Josephson junctions with a TaNx barrier for nonlatching logic applications," Appl. Phys. Lett. **78**, 99 (2001).

[18]K. Reichelt, W. Nellen, and G. Mair, "Preparation and compositional analysis of sputtered TaN films," J. Appl. Phys. **49**, 5284 (1978).

[19]J. Wright, C. Chang, D. Waters, F. Lüpke, R. Feenstra, L. Raymond, R. Koscica, G. Khalsa, D. Muller, H. G. Xing, and D. Jena, "Unexplored MBE growth mode reveals new properties of superconducting NbN," Phys. Rev. Mater. **5**, 024802 (2021).

[20]R. Yan, G. Khalsa, S. Vishwanath, Y. Han, J. Wright, S. Rouvimov, D. S. Katzer, N. Nepal, B. P. Downey, D. A. Muller, H. G. Xing, D. J. Meyer, and D. Jena, "GaN/NbN epitaxial semiconductor/superconductor heterostructures," Nature **555**, 183 (2018).

[21]M. Müller, R. Hoepfl, L. Liensberger, S. Geprägs, H. Huebl, M. Weiler, R. Gross, and M. Althammer, "Growth optimization of TaN for superconducting spintronics," Mater. Quantum Technol. **1**, 045001 (2021).

[22]P. Dang, G. Khalsa, C. S. Chang, D. S. Katzer, N. Nepal, B. P. Downey, V. D. Wheeler, A. Suslov, A. Xie, E. Beam, Y. Cao, C. Lee, D. A. Muller, H. G. Xing, D. J. Meyer, and D. Jena, "An all-epitaxial nitride heterostructure with concurrent quantum Hall effect and superconductivity," Sci. Adv. **7**, eabf1388 (2021).